Environmental Science & Technology

Article

pubs.acs.org/est

Secondary Organic Aerosol Formation from Acyclic, Monocyclic, and Polycyclic Alkanes

James F. Hunter, Anthony J. Carrasquillo, Kelly E. Daumit, and Jesse H. Kroll*

Massachusetts Institute of Technology, Cambridge, Massachusetts 02139, United States

ABSTRACT: A large number of organic species emitted into the atmosphere contain cycloalkyl groups. While cyclic species are believed to be important secondary organic aerosol (SOA) precursors, the specific role of cyclic moieties (particularly for species with multiple or fused rings) remains uncertain. Here we examine the yields and composition of SOA formed from the reaction of OH with a series of C10 (cyclo)alkanes, with 0−3 rings, in order to better understand the role of multiple cyclic moieties on aerosol formation pathways. A chamber oxidation technique using high, sustained OH radical concentrations was used to simulate long reaction times in the atmosphere. This aging technique leads to higher yields than in previously reported chamber experiments. Yields were highest for cyclic and polycyclic precursors, though yield exhibited little dependence on number of rings. However, the oxygen-to-carbon ratio of the SOA was highest for the polycyclic precursors. These trends are consistent with aerosol formation requiring two generations of oxidation and 3−4 oxygen-containing functional groups in order to condense. Cyclic, unbranched structures are protected from fragmentation during the first oxidation step, with C−C bond scission instead leading to ring opening, efficient functionalization, and high SOA yields. Fragmentation may occur during subsequent oxidation steps, limiting yields by forming volatile products. Polycyclic structures can undergo multiple ring opening reactions, but do not have markedly higher yields, likely due to enhanced fragmentation in the second oxidation step. By contrast, C−C bond scission for the linear and branched structures leads to fragmentation prior to condensation, resulting in low SOA yields. The results highlight the key roles of multigenerational chemistry and susceptibility to fragmentation in the formation and evolution of SOA.

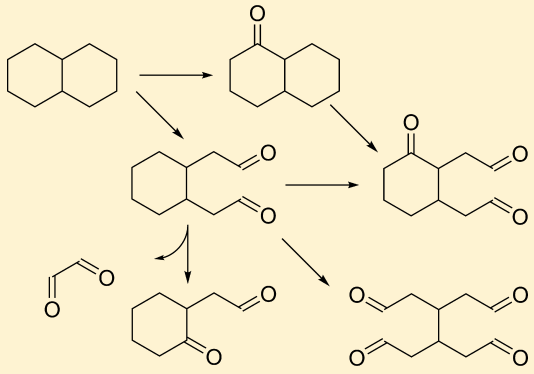

INTRODUCTION

A significant fraction of all hydrocarbons emitted into the atmosphere have molecular structures with cyclic moieties; these include cycloalkanes, aromatic species, and most mono- and sesquiterpenes. Many such species are known to be efficient precursors of secondary organic aerosol,[1−6] and thus may play an important role in air quality and climate. The role of cyclic moieties on SOA formation has been the focus of several recent studies, which find that cycloalkanes exhibit enhanced aerosol yields relative to linear alkanes of the same carbon number.[2−5] However, such studies have focused primarily on monocyclic alkanes, whereas multiple (and even fused) rings are a common structural feature in atmospheric organic species. Cyclic structures are abundant in diesel fuel and lubricating oil, with particulate organics in diesel exhaust consisting of approximately 30% monocyclic and 50% polycyclic alkanes.[7,8] Polycyclic species are also likely to be present in other industrial and combustion emissions. However, SOA formation from polycyclic alkanes has received very little laboratory study, and the effect of multiple, fused rings on SOA chemistry remains uncertain.

Figure 1 shows the classes of reaction available to unbranched acyclic, monocyclic and polycyclic alkanes in the gas phase, including functionalization (addition of oxygen-containing functional groups) and carbon−carbon bond (C−C) scission. For acyclic structures, C−C scission causes fragmentation, forming two smaller compounds (path 1b). For cyclic alkanes, the free ends of C−C scission products remain tethered together (path 2b).[2,4,9] This prevents fragmentation and leads to more functional groups on the single product, thereby promoting the formation of low-volatility species which can condense into the particle phase (and subsequently undergo oligomerization reactions[2]). Polycyclic compounds with n fused rings can resist up to n fragmentation reactions in this way (paths 3b and 3e). However, polycyclic alkanes differ from monocyclic alkanes in that their scission products are substituted rings (with functionalized alkyl substituents on the ring) rather than unbranched structures (path 3b versus 2b). These substituted rings may undergo enhanced fragmentation (path 3f), similar to the enhanced fragmentation of branched alkanes relative to linear alkanes.[2,3,5,10] Some work has examined the importance of the initial ring opening for monocyclic alkanes (path 2a versus 2b),[2] but not to our knowledge for polycyclic alkanes. The branching for later-generation oxidation pathways (2c-2e and 3c-3h) also remains highly uncertain.

Received: June 2, 2014
Revised: July 30, 2014
Accepted: August 5, 2014
Published: August 5, 2014

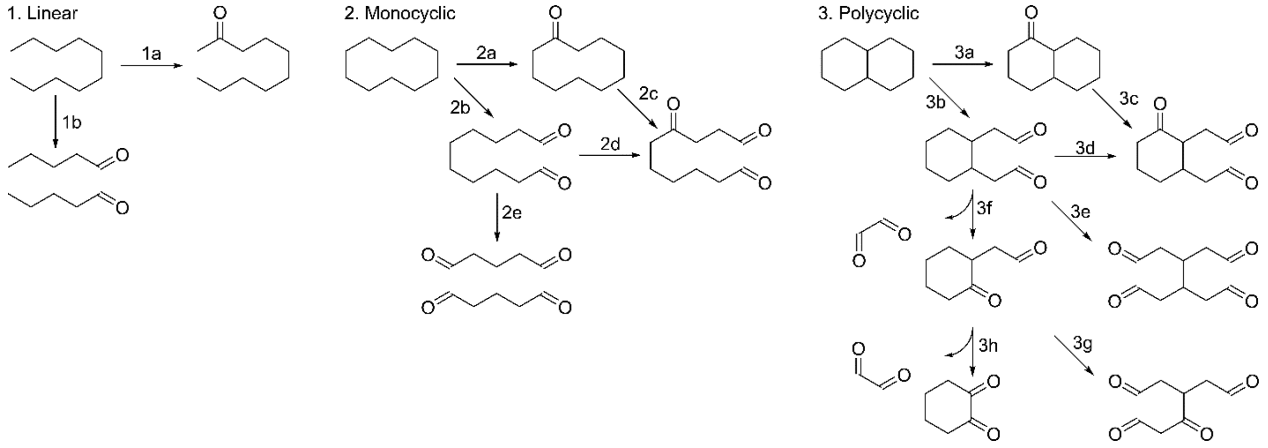

Figure 1. An illustration of different reaction pathways available to unbranched acyclic, monocyclic, and polycyclic alkanes. All arrows represent OH oxidation steps, with horizontal arrows corresponding to functionalization, diagonal arrows to C−C scission with "tethering," and vertical arrows to C−C scission with fragmentation of the carbon skeleton. For simplicity, all OH oxidation reactions are shown adding carbonyl groups to the carbon skeleton (one for functionalization, two for C−C scission). Additional fragmentation and functionalization reactions of the product species (omitted for clarity) can also occur, as can oligomerization reactions following condensation.

Table 1. Key Properties of Molecules in This Study

Name	Alkane Type	Structure	Formula	Vapor Pressure at 298 K (Pa)[a]	k_{OH}[b] (cm^3 $molecule^{-1}$ sec^{-1})	Ring Strain[c] (kJ mol^{-1})
Decane	Acyclic		$C_{10}H_{22}$	191	1.10×10^{-11}	N/A
Cyclodecane	Monocyclic		$C_{10}H_{20}$	74	1.59×10^{-11}	53
Decalin	Bicyclic		$C_{10}H_{18}$	163	1.88×10^{-11}	1.3 (trans); 12 (cis)
Pinane	Bicyclic, Substituted		$C_{10}H_{18}$	292	1.24×10^{-11}	>110[d]
JP-10	Tricyclic		$C_{10}H_{16}$	263	1.06×10^{-11}	95
Adamantane	Tricyclic		$C_{10}H_{16}$	230	2.15×10^{-11}	18-28

[a]Estimated from MPBPWIN, a component of EPI Suite.[11] [b]Atkinson et al 2003.[10] [c]Atkinson et al 1983.[12] [d]Lower-limit ring strain from four membered ring.[13]

The goal of this study is to investigate the oxidation chemistry of cycloalkyl structures and to determine the effect of additional rings on SOA formation, and specifically the relative importance of ring opening, fragmentation, and addition of functional groups. We report the aerosol yields and chemical properties for the reaction of the hydroxyl radical (OH) with a set of C10 alkanes that have zero to three rings. The role of branched cycloalkanes has been studied previously,[2,5] and is not examined here in great detail (only one such structure is included in the study) because of the present focus on the effect of additional rings. Experiments are conducted at high organic aerosol concentrations (c_{OA}) in order to increase sensitivity to more volatile products, and at high OH exposures to include the effects of oxidative aging The aim of this study is not to provide detailed yields for individual molecules, but rather to use SOA yields and composition to constrain the various reaction channels shown in Figure 1, and to better understand how such channels relate to SOA formation.

MATERIALS AND METHODS

The C10 compounds used in this study are shown in Table 1 along with their key properties. They include *n*-decane (no rings, $C_{10}H_{22}$, Sigma-Aldrich, ≥99%), cyclodecane (1 ring, $C_{10}H_{20}$, Sigma-Aldrich, 95%), decalin (bicyclo[4.4.0]decane, 2 rings, $C_{10}H_{18}$, Sigma-Aldrich, cis + trans, 99%), pinane (2,6,6-trimethylbicyclo[3.1.1]heptane, 2 rings, $C_{10}H_{18}$, Santa Cruz Biotech, endo + exo, ≥99%), JP-10 (tricyclo[5.2.1.$0^{2,6}$]decane, 3 rings, $C_{10}H_{16}$, TCI America, ≥94%), and adamantane (tricyclo[3.3.1.$1^{3,7}$]decane, 3 rings, $C_{10}H_{16}$, Sigma-Aldrich, ≥99%).

All experiments were conducted in a 7.5 m^3 environmental ("smog") chamber constructed of 0.005 in. thick perfluoroalkoxy (PFA) Teflon film (Ingeniven). The chamber is housed

in an environmental room that maintains a constant temperature of 15−40 °C. All experiments in this study were conducted at 20 °C and RH <10% (measured by a Vaisala HMP50 probe). The chamber is flanked by two sets of 24 40-W blacklights (Sylvania BL350 eco). The lamps have a standard 300−400 nm spectrum, centered at 350 nm. Full lamp intensity was used for all experiments, resulting in a J_{NO2} of ∼0.12 min^{-1}. The chamber is operated in a constant-volume ("semi-batch") mode in which clean air (Aadco 737A/C) is continuously added to make up for instrument sample flow. The lack of chamber deflation allows for relatively long (∼6−12 h) experiments at a constant surface-to-volume ratio (and therefore an approximately constant wall loss rate). Pressure in the chamber, measured with a pressure transducer (Omega Engineering), is maintained at 20−30 mTorr above the ambient atmospheric pressure. When the excess pressure exceeds 30 mTorr, a valve is automatically opened to a vacuum pump until it drops to 20 mTorr, ensuring a constant volume. The continuous addition of 5 L per minute (LPM) of clean air produces a constant dilution lifetime of 25 h, in agreement with measured dilution lifetimes of 22.4 to 24.0 h (determined from GC measurements, as described below).

Prior to each experiment, ammonium sulfate particles (serving as condensation nuclei), hexafluorobenzene (HFB, the dilution tracer), HONO (the oxidant precursor), and the precursor hydrocarbon were added to the chamber. Seed particles were atomized from a 2 g/L solution of reagent-grade ammonium sulfate (Aldrich) for 15−25 min. This produced a number-weighted average diameter of 200 nm, number concentration of 25 000−50 000 cm^{-3} and mass concentration of 50−100 $\mu g/m^3$. Hydrocarbons (∼40 ppb) and HFB (60 ppb) were added through a silicone septum into a 4 LPM flow through a coated stainless steel line (Silcotek Sulfinert) heated to 50 °C in order to aid evaporation.

The experiments used photolysis of nitrous acid (HONO) as an OH source. HONO was generated in a bubbler containing 25 mL of 1 M sodium nitrite by adding 1 M sulfuric acid via a syringe pump (Chemyx Fusion 100). The HONO produced escapes to the 1 LPM air stream of the bubbler and is sent into the chamber. An initial HONO concentration of ∼50 ppb was achieved in the chamber by adding 7.6 μL of sulfuric acid 30 min prior to initiating photochemistry. This was followed by adding ∼2 ppb per minute (0.33 μL acid per minute) once the lights were turned on to maintain a constant OH concentration. OH concentrations and exposures were estimated from hydrocarbon concentrations and OH rate coefficients using methods similar to Barmet[14] (described below). These methods indicate that the average OH concentration remains high (8.3×10^6 to 2.6×10^7 molecules/cm^3) for at least as long as the hydrocarbon remains measureable. This is typically the case for the first half of the experiment; the OH concentration is likely to remain approximately constant thereafter.[14,15]

Mass concentration and elemental composition of particles were measured using an Aerodyne high-resolution time-of-flight aerosol mass spectrometer (HR-ToF-AMS).[16,17] NO^+ and NO_2^+ (from organic nitrates) were not added to the AMS organic mass or O/C measurements in order to maintain comparability of yield data to previous work. These ions were however included in the calculation of the nitrogen-to-carbon ratio in order to provide an estimate of organic nitrate abundance. For this calculation the relative ionization efficiency of the nitrate ions was set to 1.1 rather than the value of 1.4 used for organic mass. Particle number and volume were measured using a scanning mobility particle sizer (SMPS, TSI, Inc.). Concentrations of hydrocarbon precursors and dilution tracers were measured with gas chromatography-flame ionization detection (SRI). Other measurements include ozone by UV absorption (2B Tech) and NO/NO_X by chemiluminescence (Horiba Inc.).

The correction of particle mass concentration for wall loss and dilution follows the methods of Hildebrandt et al (2009).[18] Loadings are corrected using both the organic-to-sulfate method ("AMS case 2") and the decay-rate method ("SMPS case 1"). The organic-to-sulfate method involves multiplying the time-dependent organic-to-sulfate ratio measured by the AMS by the initial sulfate mass concentration (measured by the SMPS) to produce a corrected organic mass concentration. This accounts for loss of particles to the walls, loss of vapors via equilibration with such particles (with no mass-transfer limitation), and dilution of the chamber, but not for loss of vapors to the walls themselves. As discussed in the Results section below, loss of vapors to the walls does not appear to be a dominant process for the present experiments, and thus this approach provides an upper limit for calculating organic mass.[18] The decay-rate method involves correcting aerosol mass using the particle mass loss rate (which includes wall losses and dilution), determined from 30 to 60 min of SMPS data once dilution flow is stable (after the addition of all reagents). This rate is used to separate the sulfate and organic contributions to the SMPS volume using the density of ammonium sulfate (1.77 g/cm^3) and an assumed SOA density of 1.4 g/cm^3. The corrected organic mass concentration is found by integrating the product of the particle loss rate with the suspended concentration and adding this loss term to the suspended concentration. This method assumes no partitioning of suspended vapors to the walls, and is a lower limit for estimating organic mass.[18]

SOA yields (Y) were calculated via eq 1,

$$Y = \frac{\Delta c_{OA}}{\Delta HC} \quad (1)$$

in which Δc_{OA} is the wall-loss and dilution-corrected change in total organic aerosol concentration and ΔHC is the mass concentration of hydrocarbon lost to reaction with OH. Hydrocarbon concentrations were obtained by fitting GC-FID measurements (25 min resolution) with an exponential decay and interpolating onto the timebase of the AMS (2 min). The amount of hydrocarbon lost to OH reaction is determined from eq 2,

$$\Delta HC = \Delta HC_T \times \frac{k_r}{k_r + k_d} = \Delta HC_T \times \frac{k_t - k_d}{k_t} \quad (2)$$

where ΔHC_T is the total decrease in hydrocarbon, k_d is the dilution rate, k_r is the OH reaction loss rate, and k_t is the total loss rate.

The chamber was cleaned between experiments by flushing with 35 LPM clean air at 40 °C overnight. Blank experiments were run at regular intervals to check for background aerosol. The blank experiments used an identical methodology except that the hydrocarbon precursor was omitted. These experiments produced less than 1 $\mu g/m^3$ of SOA, suggesting a negligible background effect on aerosol yields and properties. To investigate the possible effect of chamber history on SOA composition and yield, a back-to-back repeat experiment was conducted using cyclodecane. The yield increased by a factor of

1.075 and O/C decreased by a factor of 1.074 for the second experiment relative to the first. These magnitudes are on the order of typical experimental variability (~10%), suggesting that carryover does not play a major role in the results. In some cases gas-phase ammonia (50−500 ppb) was added to the chamber at the conclusion of an experiment to scavenge gas phase acids, thereby possibly suppressing organic background aerosol in the following day's experiment; this had no noticeable effects on reported yields or O/C values.

The continual addition of HONO leads to NO_X concentrations that start low but increase roughly linearly in the chamber over time, producing NO and NO_X levels of up to 240 and 475 ppb respectively. The effect of such high levels of NO_X on the SOA chemistry was assessed by performing experiments with 500 ppb of added NO. This had no measureable effect on the aerosol O/C and increased the maximum yield by a factor of 1.087 for cyclodecane; these effects are again within typical experimental variability, suggesting the NO_X addition did not have a major effect on results, and that the RO_2 chemistry is dominated by reaction with NO in the present experiments.

RESULTS AND DISCUSSION

Aerosol Formation and Yields. Figure 2 shows key time traces for a typical experiment (43 ppb cyclodecane): cycloalkane concentration, organic and sulfate mass loadings, and the organic mass loadings corrected by the organic-to-sulfate (upper limit) and decay-rate (lower limit) approaches described above. AMS O/C, H/C, and N/C are also shown, and are discussed in a later section. Initially sulfate signal decays due to wall losses, then sharply increases as organics condense onto the sulfate seeds and increase the AMS collection efficiency.[19] The corrected organic loading increases rapidly and eventually levels off, marking the point where the maximum SOA yield has been achieved (at an OH exposure of 1.1×10^8 molecules cm^{-3} hr). The two correction methods diverge with time and lead to significantly different final concentrations; these differences are substantially larger in the present experiments than in previous studies[18] because aerosol production is sustained over a longer time (6−10 h) than in typical chamber experiments (1−4 h).[2,4,18,20] The disparity between the wall loss correction methods dominates the overall uncertainty in yields (the measurement errors are on the order of 10%), underlining the importance of future research aimed at better quantifying losses of particles and vapors to the chamber walls.

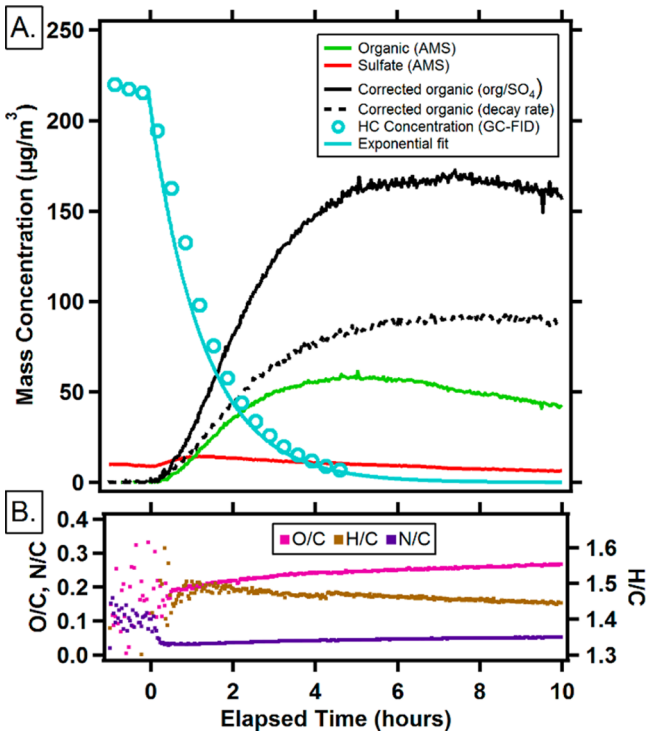

Figure 2. Time traces for key measurements during a typical experiment (oxidation of cyclodecane). Photochemistry is initiated at $t = 0$. Panel A: Cycloalkane concentrations, AMS measurements of organic and sulfate aerosol, and corrected aerosol loading measurements. AMS mass loadings are not corrected for collection efficiency (CE), but corrected loadings take into account wall loss, dilution and changes to CE. Panel B: Elemental ratios.

Table 2 summarizes yield results for all experiments, with maximum SOA yields versus c_{OA} shown in Figure 3. The c_{OA} ranges from 80 to 300 $\mu g/m^3$; this is higher than typical atmospheric levels but enables precise measurements of the aerosol composition without necessitating complex background subtraction procedures.

Comparison with Previous Results. Results from previous SOA studies of C10 species are also given in Table 2. Chamber studies of SOA have previously been made for *n*-decane[2,20] and cyclodecane,[2,4] but not for any of the other compounds in this study. For the chamber studies,[4,20] volatility basis set (VBS) fits (for $c^* = 0.1$ to 100 $\mu g/m^3$) are given in Figure 3.[21] Extrapolations to higher c_{OA} are also shown (dashed lines), but these are highly uncertain.[22] More volatile material ($c^* \geq 1000$ $\mu g/m^3$) may contribute SOA at high c_{OA}, so these extrapolations represent lower limits. Results by Lim and Ziemann[2] are not included in Figure 3 since those experiments were run at much higher organic loading. Yields for *n*-decane and cyclodecane are substantially higher here than those reported by Tkacik et al.,[4] Presto et al.[20] and Lim and Ziemann.[2] Although higher yields are expected at higher c_{OA} due to absorptive partitioning,[23] differences in c_{OA} cannot fully explain the differences between the previous chamber studies and the present work. Yields reported by Lim and Ziemann[2] are actually lower than those achieved here despite the much higher organic loading in those experiments. The differences in yields can instead be explained by differences in OH exposures (given in Table 2). The OH exposures in this work, required in order to reach maximum SOA yields, are up to a factor of 25 higher than comparable chamber experiments. This suggests that the yields and properties reported here are more representative of SOA formed after substantial aging (multiple days in the atmosphere) than those reported in previous chamber studies.

By contrast, the measured yields for *n*-decane are lower than those measured in the flow-reactor experiments of Lambe et al.[24] (also included in Figure 3 and Table 2), and yields from JP-10 are in reasonable agreement with the results from that study. Those experiments were carried out under NO_X-free conditions, with higher OH concentrations (8×10^8 to 2×10^{10} molecules/cm^3) and much shorter residence times (100 s) than the chamber experiments. Yields were corrected for wall loss using the measured size-dependent particle transmission efficiency of the flow reactor.[24] This method does not include losses of vapors to wall-bound particles and is most similar to the decay-rate correction method. The OH exposures were higher than in the present chamber study, but only by a factor

Table 2. Yields and Elemental Composition of SOA from C10 Compounds[a]

compound	% SOA yield (mass) upper[b]	% SOA yield (mass) lower[c]	% SOA yield (carbon) upper[b]	% SOA yield (carbon) lower[c]	c_{OA} ($\mu g/m^3$) upper[b]	c_{OA} ($\mu g/m^3$) lower[c]	O/C[e]	H/C[e]	N/C[e]	DBE[f]	excess DBE[f]	OH exposure (molec/cm^3·hr)
***n*-Decane**												
this study	25.4	9.6	19.6	7.4	91.4	23.4	0.33	1.58	0.031	3.1	0	4.5×10^7
Presto[20]	1.5	–	–	–	6	–	–	–	–	–	–	1.2×10^7
Lim[2]	-	14.6	–	–	–	828	–	–	–	–	–	2.9×10^7
Lambe[24]	-	39[d]	–	29[d]	–	231[d]	0.35	1.53	–	3.3	0.2	1.4×10^8
Cyclodecane												
this study	147	60.3	115	47.2	302	84.3	0.28	1.47	0.054	3.6	0.5	1.6×10^8
this study	137	86.2	104	65.4	282	114	0.28	1.48	0.049	3.6	0.5	9.6×10^7
this study	148	96.4	111	72.3	294	118	0.33	1.42	0.043	3.9	0.8	8.5×10^7
Tkacik[4]	25	–	17	–	15	-	0.30	1.34	–	4.3	1.2	6.0×10^6
Lim[2]	–	64.1	–	–	–	3325	–	–	–	–	–	7.7×10^6
Decalin												
this study	138	113	98.3	88.5	296	131	0.35	1.38	0.045	4.1	1.0	2.4×10^7
Pinane												
this study	39.6	38.0	24.6	23.6	89.0	44.2	0.53	1.31	0.050	4.4	1.3	5.4×10^7
JP-10												
this study	181	138	125	95.3	383	149	0.39	1.33	0.046	4.3	1.2	9.1×10^7
this study	173	83.8	130	62.9	359	167	0.34	1.30	0.047	4.5	1.4	1.6×10^8
Lambe[24]	–	110[d]	–	72[d]	–	306[d]	0.74	1.22	–	4.9	1.8	2.6×10^8
Adamantane												
this study	114	99.0	77.1	67.0	238	142	0.42	1.26	0.064	4.7	1.6	5.2×10^7

[a]Quantities that were not measured/reported in previous studies are denoted with a "–" [b]Yields computed using organic-to-sulfate wall loss correction method. [c]Yields computed using decay-rate wall loss correction method assuming an SOA density of 1.4 g/cm^3. [d]Maximum yields measured from oxidation within a flow reactor, corrected for wall loss using methods detailed in Lambe et al.[24] [e]Determined from W-mode AMS data from the final hour of each experiment, associated with the maximum SOA yield achieved. N/C includes NO^+ and NO_2^+ and therefore provides a measure of organic nitrate abundance. [f]Double Bond Equivalents, computed from eq 2 assuming condensed-phase products retain all 10 carbon atoms. "Excess DBE" computed by subtracting 3.1 from the DBE to account for carbonyl functionalities.

of ~3. That the yields in the present study agree more closely with the flow-reactor study than previous chamber studies again suggests the importance of multigenerational oxidation in SOA formation. However, differences in reaction conditions (e.g., NO_X level, irradiation) make it difficult to directly compare results from the two experiments.

Figure 3 shows yields computed using both the organic-to-sulfate (upper limit) and decay-rate (lower limit) correction methods. These limits diverge over a given experiment, as shown in Figure 2, so that uncertainty in organic aerosol concentration and yield increases with time (and hence degree of aging). The mass yields may be constrained further by carbon yields, computed from the mass yields and the mass fraction carbon determined from AMS elemental analysis data. The upper-limit and lower-limit carbon yields for this study are given in Table 2. In many cases the upper-limit carbon yields are above the strict maximum of 100%, indicating that the organic-to-sulfate method is an overestimate (by up to 30%). Such high carbon yields imply that losses to the chamber walls (either to wall-bound particles or to the Teflon itself) are not a dramatic sink of organic vapors in the present experiments, in contrast to chamber studies of other SOA-forming systems.[25,26]

Influence of Number of Rings on Yields and Mechanisms. All cyclic species (except pinane) have a substantially higher SOA yield than *n*-decane; this is consistent with previous results[2,4,20,24] and can be explained by the "tethering" effect discussed above. However, no clear additional increase in yield is observed as the number of rings increases beyond one. This lack of dependence on ring number may arise from differences in multigenerational oxidation pathways for monocyclic and polycyclic alkanes, as illustrated in Figure 1. C−C scission of monocyclic species (pathway 2b) results in an acyclic product with terminal oxygen-containing functional groups. The high yield indicates that fragmentation (2e) does not occur to a major extent, and/or that it is associated with minimal carbon loss. For polycyclic alkanes, C−C scission results in substituted cyclic structures (e.g., the product of pathway 3b). These structures likely fragment more than in the monocyclic case (3f is enhanced relative to 2e), much like branched alkanes fragment more readily than linear alkanes.[2,3] This likely also explains the low yield of pinane, which has a branched starting structure analogous to the product of 3b; this effect may also be relevant to other branched cyclic species as well. However, enhanced fragmentation for polycyclic species may be offset by additional ring opening pathways (3g), ultimately leading to comparable yields for monocyclic and polycyclic compounds. As discussed below, the elemental ratios of the SOA provide additional evidence for the enhanced ring opening of polycyclic compounds and increased fragmentation of ring-opened products.

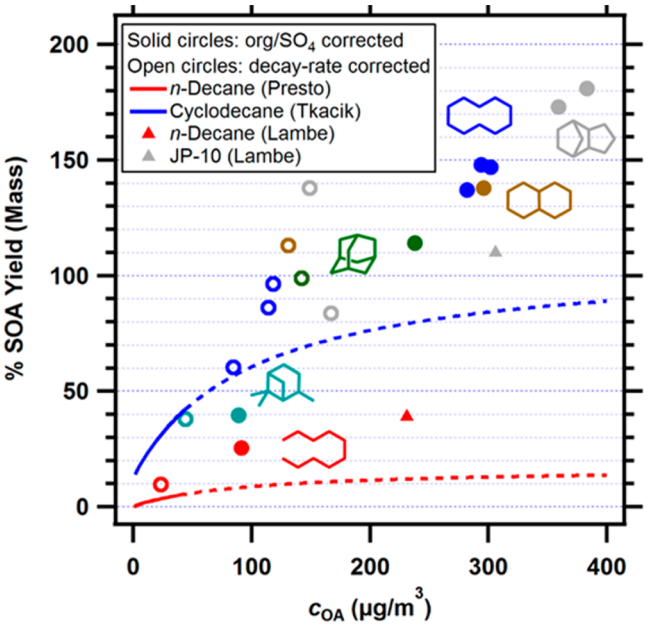

Figure 3. Yields of organic aerosol computed using both the organic-to-sulfate (closed circles) and decay-rate (open circles) correction methods, and comparison with previous yield measurements (lines and triangles). Color denotes SOA precursor (red: *n*-decane; dark blue: cyclodecane; brown: decalin; light blue: pinane; green: adamantane; gray: JP-10). VBS fits of *n*-decane and cyclodecane mass yields from Presto et al.[20] and Tkacik et al.[4] are shown, with extrapolated fits indicated by dashed lines. The maximum reported yields of *n*-decane and JP-10 from the flow-tube study of Lambe et al.[24] are also shown (triangles). Overall uncertainties in yields is dominated by differences between lower limit and upper limit wall loss corrections rather than uncertainty in the measurement techniques (~10%).

Once product vapor pressure is sufficiently low to condense, the oxidation rate slows significantly due to the "trapping" effect, in which species are protected from further oxidation due to partitioning into the condensed phase. Heterogeneous oxidation may still occur, but is much slower that gas-phase oxidation.[9,27,28] The "trapping point" depends on the volatility of the products, the aerosol loading, and the extent to which the condensed-phase products rapidly form oligomers. The uniformly high SOA yields for all unbranched polycyclic compounds suggest that under the conditions of this study (high aerosol loading), trapping follows the second generation of oxidation, since if further oxidation were to occur, there would likely be differences in the yields of the monocyclic and polycyclic compounds. For example, a third oxidation step for cyclodecane would likely result in fragmentation, because second-generation products are likely to be ring-opened and functionalized. For polycyclic species, although the remaining rings are less effective at preventing fragmentation once the first ring has opened, some "tethering" may still occur, increasing the yield of lower volatility products relative to a structure with no remaining rings. Thus, gas-to-particle conversion after two generations of oxidation leads to similar yields for all cyclic structures examined in this study; however, differences might emerge if further oxidation is possible. This could result either from lower aerosol loadings or decreased carbon number of the precursors. At lower loadings, products must have a lower volatility to partition into the condensed phase, potentially requiring additional oxygenated functional groups and therefore additional oxidation steps. Similarly, compounds with lower carbon numbers start with a higher volatility, and require a larger number of oxidation steps to achieve the same low volatility as a larger compound. In either case, the more oxidation steps that take place, the less effective rings are expected to be in producing high SOA yields, since fragmentation should increase on increasingly ring-opened and oxygenated structures.

The carbon yields in Table 2 help to further constrain the relative importance of the multigenerational fragmentation pathways. The upper limit carbon yields for the cyclic, unbranched structures are 77−130%, while lower limit carbon yields are 47−95%. The carbon yields, like the mass yields, do not vary with number of rings. The fraction of remaining gas-phase carbon (0−53%) suggests that fragmentation occurs somewhat for the cyclic alkanes, and is not necessarily prevented by the presence of multiple rings. However this fraction is generally small, suggesting that fragmentation (e.g., pathways 2e, 3f, and 3h) is a relatively minor channel for the cyclic structures under the conditions of this study (high aerosol loading, 10 carbon atoms per precursor). Conversely, the larger fraction of carbon present in the gas phase for linear or branched compounds (75−93%) suggests that fragmentation dominates overall gas-phase reactivity for such species. Fragmentation is unlikely in the first oxidation step for linear alkanes,[2,3,10] and instead likely dominates in later generations, as expected for oxygenated species.[29]

Lim and Ziemann[2] previously explained the high yields of monocyclic alkanes in terms of the relative probability of C−C scission and isomerization/functionalization (e.g., path 2a versus 2b in Figure 1). In that analysis, greater ring strain energy increases C−C scission for cyclic alkanes. This scission results in ring-opened products that are multifunctional and possibly subject to enhanced oligomer formation,[2] and thereby increases aerosol yield. No trend in yield with ring strain (given in Table 1) is apparent in the present study, suggesting that the probability of ring opening in the first oxidation step does not govern SOA formation. Instead, it appears that multiple generations of oxidation are required, reducing the relative importance of any individual ring opening step. Furthermore, ring strain is expected to change over a multigenerational oxidation process. Functionalized rings have increased ring strain[13] which may increase the likelihood of ring opening in subsequent oxidation steps.

Role of Number of Rings on SOA Elemental Composition. Aerosol elemental ratios (averaged over the final hour of each experiment) are given in Table 2. Typical time traces for O/C, H/C, and N/C are also shown in panel B of Figure 2; changes in these ratios are relatively minor despite significant changes in loading and OH exposure. The O/C for SOA from all precursors (except pinane) ranges from ~0.3 to ~0.4, indicating that a 10 carbon skeleton acquires 3−4 oxygen atoms before reaching a low enough volatility to condense at the loadings in the present study. Since each oxidation step is likely to add 1−2 functional groups, this is consistent with the second oxidation step leading to SOA formation. O/C increases slightly with increasing ring number. This suggests enhanced ring opening, since this reaction channel adds more functional groups per oxidation step. The relatively unchanging O/C implies little oxidation of condensed-phase organic species, consistent with slowed oxidation due to "trapping" after these two steps. The high O/C of pinane is an exception, likely due to increased fragmentation; fragmentation products

have a reduced carbon number and are more volatile, leading to both reduced yields and increased O/C.

Aerosol organic nitrogen is entirely due to NO^+ and NO_2^+ such that the abundance of organic nitrates can be inferred from the N/C values given in Table 2. Assuming that the oxidation products in SOA retain all 10 carbon atoms, the organic nitrate yield ranges from 31% to 64%. Because the maximum nitrate yield for a single reaction step is expected to be approximately 30%,[30] this suggests multiple oxidation steps are required. Nitrate yields appear to be systematically higher for all the cyclic compounds, but do not exhibit a trend with increasing ring number. Inclusion of nitrate in the organic mass increases aerosol mass by an additional 10 to 20%, but would not affect any of the overall trends or conclusions of this work.

The relative importance of functionalization and ring-opening reactions in the oxidation of the cyclic alkanes can be constrained by the average number of double bond equivalents (DBE) of the molecules within the SOA, calculated via

$$\mathrm{DBE} = n_C + 1 - \frac{n_H}{2} = 1 + n_C\left(1 - 1/2\frac{H}{C}\right) \quad (3)$$

in which n_C and n_H are the number of carbon atoms and hydrogen atoms in an average molecule. Calculated DBE values are given in Table 2; we assume that n_C = 10 (i.e., SOA contains no fragmentation products), though small decreases in n_C do not strongly affect DBE values. Carbon−carbon double bonds are unlikely to be stable under the highly oxidizing conditions of the present experiments, suggesting the DBE is roughly equal to the total number of intact rings and carbonyl functionalities. The DBE of *n*-decane SOA indicates that, on average, 3.1 carbonyl groups are added to each carbon skeleton; the remaining functional groups involve C−O single bonds. Assuming that the SOA functional group distribution is similar for all precursors studies, the number of retained rings can be approximated from the "excess DBE" (equal to DBE − 3.1). By comparing this to the number of rings that each molecule started with, the average number of ring opening reactions that the SOA components have undergone can be estimated: 0.2−0.5 for cyclodecane, 0.7−1.0 for the bicyclic compounds, and 1.4−1.8 for the tricyclic compounds. Although these values are only approximate, due to differences in functional group distribution (and possibly the importance of oligomerization[2]), there is a clear increasing trend in the degree of ring opening with number of rings. Were additional oxidation steps to occur (e.g., at lower loadings or carbon number), additional ring opening might be expected to occur.

Consistent with the yield measurements, the elemental ratio measurements point to the ubiquity of ring opening for all the cyclic structures, and the importance of both additional ring opening and fragmentation in polycyclic moieties over the multiple generations of oxidation required to form SOA in these experiments. Although "tethering" implies that a polycyclic compound with *n* rings can resist up to *n* C−C bond scissions without fragmenting, in practice fragmentation of early-generation products may be important, since the first ring-opening product has a branched structure. For pinane, a precursor that has both rings and branches, this competition exists in the first oxidation step, leading to lowered yields. Finally, unbranched monocyclic compounds comprise a special case in which ring opening results in a linear molecule with primary oxygenated functional groups, with little fragmentation of gas-phase products. The yield and chemical composition measurements show that aerosol formation from cyclic compounds is a multigenerational process, and that the degree of fragmentation (which is a strong function of molecular structure) is critical to the amount and properties of the aerosol that is eventually formed.

AUTHOR INFORMATION

Corresponding Author

*Phone: (617) 253-2409; e-mail: jhkroll@mit.edu.

Notes

The authors declare no competing financial interest.

ACKNOWLEDGMENTS

This work was supported by the National Science Foundation, under grant number AGS-1056225.

REFERENCES

(1) Griffin, R. J.; Cocker, D. R.; Flagan, R. C.; Seinfeld, J. H. Organic aerosol formation from the oxidation of biogenic hydrocarbons. *J. Geophys. Res.* **1999**, *104*, 3555−3567.

(2) Lim, Y. B.; Ziemann, P. J. Effects of molecular structure on aerosol yields from OH radical-initiated reactions of linear, branched, and cyclic alkanes in the presence of NO. *Environ. Sci. Technol.* **2009**, *43*, 2328−2334.

(3) Ziemann, P. J. Effects of molecular structure on the chemistry of aerosol formation from the OH-radical-initiated oxidation of alkanes and alkenes. *Int. Rev. Phys. Chem.* **2011**, *30*, 161−195.

(4) Tkacik, D. S.; Presto, A. A.; Donahue, N. M.; Robinson, A. L. Secondary organic aerosol formation from intermediate-volatility organic compounds: Cyclic, linear, and branched alkanes. *Environ. Sci. Technol.* **2012**, *46*, 8773−8781.

(5) Yee, L. D.; Craven, J. S.; Loza, C. L.; Schilling, K. A.; Ng, N. L.; Canagaratna, M. R.; Ziemann, P. J.; Flagan, R. C.; Seinfeld, J. H. Effect of chemical structure on secondary organic aerosol formation from C12 alkanes. *Atmos. Chem. Phys.* **2013**, *13*, 11121−11140.

(6) Ng, N. L.; Kroll, J. H.; Chan, A. W. H.; Chhabra, P. S.; Flagan, R. C.; Seinfeld, J. H. Secondary organic aerosol formation from *m*-xylene, toluene, and benzene. *Atmos. Chem. Phys.* **2007**, *7*, 3909−3922.

(7) Worton, D. R.; Isaacman, G.; Gentner, D. R.; Dallmann, T. R.; Chan, A. W. H.; Ruehl, C.; Kirchstetter, T. W.; Wilson, K. R.; Harley, R. A.; Goldstein, A. H. Lubricating oil dominates primary organic aerosol emissions from motor vehicles. *Environ. Sci. Technol.* **2014**, *48*, 3698−3706.

(8) Gentner, D. R.; Isaacman, G.; Worton, D. R.; Chan, A. W. H.; Dallmann, T. R.; Davis, L.; Liu, S.; Day, D. A.; Russell, L. M.; Wilson, K. R.; et al. Elucidating secondary organic aerosol from diesel and gasoline vehicles through detailed characterization of organic carbon emissions. *Proc. Natl. Acad. Sci.* **2012**, *109*, 18318−18323.

(9) Kessler, S. H.; Smith, J. D.; Che, D. L.; Worsnop, D. R.; Wilson, K. R.; Kroll, J. H. Chemical sinks of organic aerosol: Kinetics and products of the heterogeneous oxidation of erythritol and levoglucosan. *Environ. Sci. Technol.* **2010**, *44*, 7005−7010.

(10) Atkinson, R.; Arey, J. Atmospheric degradation of volatile organic compounds. *Chem. Rev.* **2003**, *103*, 4605−4638.

(11) U.S. EPA. *Estimation Programs Interface Suite™ for Microsoft® Windows 8*, 2014.

(12) Atkinson, R.; Aschmann, S. M.; Carter, W. P. L. Rate constants for the gas-phase reactions of OH radicals with a series of bi- and tricycloalkanes at 299 ± 2 K: Effects of ring strain. *Int. J. Chem. Kinet.* **1983**, *15*, 37−50.

(13) Benson, S. W. *Themochemical Kinetics*, 2nd ed.; Wiley Interscience, 1976.

(14) Barmet, P.; Dommen, J.; Decarlo, P. F.; Tritscher, T.; Praplan, A. P.; Platt, S. M.; Prévôt, A. S. H.; Donahue, N. M.; Baltensperger, U. OH clock determination by proton transfer reaction mass spectrometry at an environmental chamber. *Atmos. Meas. Tech.* **2012**, *5*, 647−656.

(15) Pfaffenberger, L.; Barmet, P.; Slowik, J. G.; Praplan, A. P.; Dommen, J.; Prévôt, A. S. H.; Baltensperger, U. The link between organic aerosol mass loading and degree of oxygenation: An α-pinene photooxidation study. *Atmos. Chem. Phys.* **2013**, *13*, 6493−6506.
(16) Decarlo, P. F.; Kimmel, J. R.; Trimborn, A.; Northway, M. J.; Jayne, J. T.; Aiken, A. C.; Gonin, M.; Fuhrer, K.; Horvath, T.; Docherty, K. S.; et al. Field-deployable, high-resolution, time-of-flight aerosol mass spectrometer. *Anal. Chem.* **2006**, *78*, 8281−8289.
(17) Aiken, A. C.; Decarlo, P. F.; Kroll, J. H.; Worsnop, D. R.; Huffman, J. A.; Docherty, K. S.; Ulbrich, I. M.; Mohr, C.; Kimmel, J. R.; Sueper, D.; et al. O/C and OM/OC ratios of primary, secondary, and ambient organic aerosols with high-resolution time-of-flight aerosol mass spectrometry. *Environ. Sci. Technol.* **2008**, *42*, 4478−4485.
(18) Hildebrandt, L.; Donahue, N. M.; Pandis, S. N. High formation of secondary organic aerosol from the photo-oxidation of toluene. *Atmos. Chem. Phys.* **2009**, *9*, 2973−2986.
(19) Bahreini, R.; Keywood, M. D.; Ng, N. L.; Varutbangkul, V.; Gao, S.; Flagan, R. C.; Seinfeld, J. H.; Worsnop, D. R.; Jimenez, J. L. Measurements of secondary organic aerosol from oxidation of cycloalkenes, terpenes, and *m*-xylene using an Aerodyne aerosol mass spectrometer. *Environ. Sci. Technol.* **2005**, *39*, 5674−5688.
(20) Presto, A. A.; Miracolo, M. A.; Donahue, N. M.; Robinson, A. L. Secondary organic aerosol formation from high-NO_X photo-oxidation of low volatility precursors: *n*-Alkanes. *Environ. Sci. Technol.* **2010**, *44*, 2029−2034.
(21) Donahue, N. M.; Robinson, A. L.; Stanier, C. O.; Pandis, S. N. Coupled partitioning, dilution, and chemical aging of semivolatile organics. *Environ. Sci. Technol.* **2006**, *40*, 2635−2643.
(22) Stanier, C. O.; Donahue, N. M.; Pandis, S. N. Parameterization of secondary organic aerosol mass fractions from smog chamber data. *Atmos. Environ.* **2008**, *42*, 2276−2299.
(23) Odum, J. R.; Hoffmann, T.; Bowman, F. M.; Collins, D.; Flagan, R. C.; Seinfeld, J. H. Gas/particle partitioning and secondary organic aerosol yields. *Environ. Sci. Technol.* **1996**, *30*, 2580−2585.
(24) Lambe, A. T.; Onasch, T. B.; Croasdale, D. R.; Wright, J. P.; Martin, A. T.; Franklin, J. P.; Massoli, P.; Kroll, J. H.; Canagaratna, M. R.; Brune, W. H.; et al. Transitions from functionalization to fragmentation reactions of laboratory secondary organic aerosol (SOA) generated from the OH oxidation of alkane precursors. *Environ. Sci. Technol.* **2012**, *46*, 5430−5437.
(25) Zhang, X.; Cappa, C. D.; Jathar, S. H.; McVay, R. C.; Ensberg, J. J.; Kleeman, M. J.; Seinfeld, J. H. Influence of vapor wall loss in laboratory chambers on yields of secondary organic aerosol. *Proc. Natl. Acad. Sci. U. S. A.* **2014**, 1−6.
(26) Matsunaga, A.; Ziemann, P. J. Gas-wall partitioning of organic compounds in a teflon film chamber and potential effects on reaction product and aerosol yield measurements. *Aerosol Sci. Technol.* **2010**, *44*, 881−892.
(27) Smith, J. D.; Kroll, J. H.; Cappa, C. D.; Che, D. L.; Liu, C. L.; Musahid, A.; Leone, S. R.; Worsnop, D. R.; Wilson, K. R. The heterogeneous reaction of hydroxyl radicals with sub-micron squalane particles: A model system for understanding the oxidative aging of ambient aerosols. *Atmos. Chem. Phys.* **2009**, *9*, 3209−3222.
(28) George, I. J.; Abbatt, J. P. D. Chemical evolution of secondary organic aerosol from OH-initiated heterogeneous oxidation. *Atmos. Chem. Phys.* **2010**, *10*, 5551−5563.
(29) Atkinson, R. Rate constants for the atmospheric reactions of alkoxy radicals: An updated estimation method. *Atmos. Environ.* **2007**, *41*, 8468−8485.
(30) Ziemann, P. J.; Atkinson, R. Kinetics, products, and mechanisms of secondary organic aerosol formation. *Chem. Soc. Rev.* **2012**, *41*, 6582−6605.